Chapter 8

Numerical and experimental analyses of wearable antennas, including novel fabrication and metrology techniques

Isidoro Ibanez-Labiano[1], Syeda Fizzah Jilani[2], Elif Ozden-Yenigun[3] and Akram Alomainy[1]

Most fifth-generation (5G) mobile network applications require wearable antennas to be unobtrusive, low-profile, low-power and electrically small. Such antennas are a crucial element in wearable body-centric wireless system designs for delivering 5G user's experience. Wearable antennas can be employed in a wide range of applications from communicating, harvesting energy to sensing capabilities. For this purpose, fabrics and novel materials such as graphene are been explored in order to cope with the wearable device demands in terms of flexibility, conform-ability and lightweight. Similarly, novel fabrication techniques for wearable antenna prototyping such as screen printing, inkjet printing, embroidery and cutters are been investigated to exploit the unique characteristics of various materials. These innovative fabrication methods allow a high degree of fabrication precision enabling their uptake for 5G applications. Due to power absorption by lossy human body tissues, a distorted radiation pattern and lower radiation efficiency are envi-saged when they are worn on and at proximity to the body. Furthermore, when designing the antenna, the body proximity effects must be considered to prevent significant antenna detuning and the consequent mismatch. Numerical and experimental human body phantoms are used with a view to simulate its impact. This chapter presents an analysis of novel fabrication methods for wearable antennas, methodologies and measurement techniques to characterise their perfor-mance in a dynamic body-worn communication environment. This chapter delivers a review of different novel fabrication techniques for wearable antennas such as various printing processes, machine embroidery and laser methods. Follow by a metrology section, where numerical and experimental human phantoms are explained and durability tests described. Three examples of 5G wearable antennas

[1]School of Electronic Engineering and Computer Science, Queen Mary University of London, London, United Kingdom

[2]Department of Physics, Aberystwyth University, Ceredigion, United Kingdom

[3]School of Design, Textiles, Royal College of Art, London, United Kingdom

for different frequencies and their on-body performance characterisation are pro-vided. Finally, it is closed with a summary of the outcomes achieved in this chapter and future prospects of the research.

8.1 Introduction

The idea of application-specific user-body-centric wireless networks built around wearable devices and nodes placed at certain locations has significantly evolved in the past few years with them becoming integrated aspects of our daily activities for healthcare, well-being and immersive information and communication technology and entertainment experience. A significant progress has been made particularly for biometry and communication at microwave frequencies [1,2]; however, the migration of developing wireless systems towards the millimetre-wave (mm-wave) spectrum for fifth-generation (5G) and beyond is driving various research trends, including design, fabrication and measurement techniques of wearable antennas towards higher frequency bands due to the attraction over their inherent advantages on high data rates, secured links and lower probability of interference [3–6].

A number of commercial wearable devices have been introduced and available in the market; however, they are restricted to certain applications and demand more versatility, compactness and diversity [7]. A wearable antenna is often regarded as an integral part of a wireless wearable device and its performance should guarantee a satisfactory wireless communication link between the communicating nodes positioned on different parts of the human body and also with off-body units to ensure the required power transfer. The antenna solution in such application should be low-profile, compact and conformal enough to adapt to the shape and curvature of the human body, as well as easily integrate-able within garments and everyday clothing. In practice, wearable antennas may experience a resonance shift or dis-tortion in radiation characteristics when placed closer to the human body which requires high robustness to reduce the impact of the body on antenna performance [8]. It is important that the proposed antenna solutions at mm-wave should be insensitive to the effect of the body presence or at least include such effect in the design and analysis procedure to ensure efficient link performance. They must ensure high-gain characteristics to reduce node-to-node path-loss [9], which can be avoided or minimised through the use of high-gain and directional antennas. Pattern reconfiguration would provide a suitable solution, as the cognitive control on the direction of radiation can configure the shortest distance between the transmitter and receiver and enhance the link quality significantly. It is also important to ensure adaptability of radiation performance to the required commu-nication path; with the direction of maximum radiation of the antenna being tan-gential to the body surface for on-body links, while being orthogonal for off-body links [10,11].

A number of versatile mm-wave antennas consisting of conventional or novel patch geometries provided with the broadside radiation response suitable for off-body communication, or end-fire radiation for on-body links have been reported on

60 GHz. For instance, a four-element patch array is proposed on a 127-mm thin RT/duroid film with a gain of approximately 12 dBi, and a human phantom is also used for the characterisation of body effects [12]. It is observed that the effects of the phantom on the antenna performance are negligible due to broadside radiation being shielded from the body by the back-layer ground plane. The four-element antenna array is also designed and implemented on a textile substrate for off-body scenario [13]. In addition, a 60-GHz textile-based Yagi–Uda end-fire antenna fabricated by ad hoc manufacturing process is suggested for body area networks and also realised on thin substrates to demonstrated on-body communications [14,15]. The authors have led research activities to design and experimentally validate an inkjet-printed flexible leaky-wave wideband antenna array at mm-wave with the capability of limited beam-steering [16,17] and also mm-wave wearable antenna solution with significant size reduction [18], respectively. However, the major drawback of reported and presented designs in the open literature is the limited flexibility in terms of functionality and reconfiguration and also the lack of adaptability in a cognitive manner to the radio link.

Considering all the progress that has been made in the area, there are still critical challenges remain to be solved. High free-space path loss and oxygen-induced atmospheric attenuations are major challenges in the realisation of a reli-able and efficient mm-wave communication links, which require innovations and original contributions in terms of radio frequency (RF) front-end that could com-pensate for such losses and enhance the overall system performance. Although these issues might provide difficulties and obstacles in the realisation on wearable technologies at mm-wave, they could be addressed and minimised (in some cases eliminated) in efficiently designed antenna solutions. In addition, experimental characterisation of suitable arrays at mm-wave need to adhere to specific thresholds and end-user informed requirements. As an example, the human body presents a dynamic environment, specifically for wearable applications, which leads to increased signal losses due to the misalignment of communicating nodes that is, in some cases, greater than the absorption loss.

8.2   Advanced fabrication techniques for wearable antennas

Wearable antennas are a key component of wearable wireless communication systems. Such antennas are often unobtrusive, low-profile, electrically small and with low-power consumption for delivering the desired user's experience. Wearable antennas can be used for communication, energy harvesting or as sen-sors. This section presents the advances in fabrication techniques for flexible wearable antennas. Such antennas, design to be worn, have specific requirements such as flexibility, compactness, reconfigurability, conformability and durability. Therefore, the materials used and production methods in wearable antennas are quite unconventional and need to be evaluated. Recently, textile-based antennas and electronic circuitries integrated as a part of
a garment or a clothing have recently gathered huge attention [19,20]. Flexible

antennas are anticipated to have a substantial impact in the development of a numerous wireless applications for 5G and beyond. Printed devices on flexible sub-strates combine the benefits of low-cost fabrication, light-weight, thin form factor, conformity and compliance with the contours of non-planar surfaces, rollability and robustness against cracks due to stretching, bending and folding [21]. These features along with the smart packaging techniques are necessary for wearable electronics, body-centric sensors and many other future wireless applications. A high-frequency spectrum has gained substantial attention to increase the bandwidth resources for future wireless networks to accommodate a rapidly increasing number of devices and applications. This transition implies a significant reduction in the size of the antenna and other electronic components and thus requires advanced manufacturing techni-ques to fulfil the high-accuracy demands associated with the shorter wavelength.

Several efficient methods such as photolithography, inkjet printing [22–25], flexography [26] and screen printing [27,28] are famous for inexpensive mass-production of printed flexible electronics. These fabrication processes are additive growth methods and involve an automated layer-by-layer deposition or growth sequence on a substrate [29,30]. Photolithography offers high accuracy, although it involves highly sophisticated clean-room facilities to transfer a pattern on a substrate by means of light [31]. Flexible substrates with laminated metallic sheets of copper or aluminium can be prototyped with high accuracy by means of a laser milling equipment [32,33]. Inkjet printing is another method to achieve good accuracy by using a computer-aided inkjet printer and can be extended to a reel-to-reel process for a time-efficient bulk-fabrication [34,35]. Conductive embroidered patterning with conductive yarns on fabrics for antennas is also a reasonable alternative especially in wearable antennas integrated in clothing. In addition, several conductive woven fabrics can be sewed on the textile substrate as a radiating area of the antennas as well as other circuitries. Among the fast, high-resolution and cost-effective printing techniques, screen printing is promising due to simplicity, affordability, time-efficiency and reduced material wastage [36]. When compared with the expensive instruments required for the inkjet printing, laser prototyping or cleanroom condi-tions, screen printing is an appropriate choice with reasonable fabrication accuracy on a variety of substrates like plastics, fabrics, polymers, etc. Further discussion on these techniques is presented as follows.

8.2.1   Screen printing

Screen printing is a process of transferring a pattern by means of a screen or an ink-blocking stencil that defines the area to be patterned on the substrate using a paste. Conductive pastes and metallic epoxies are widely used in this regard to pattern conductive lines, pads and metallic structures for the printable electronics and antennas by using the screen printing process. A number of variants are commer-cially available such as micro/nanoparticle conductive inks, pastes and epoxies based on variation in the composition, wettability, adhesion and conductivity. The conductivity of these pastes is mainly dependent on the concentration of the metal particles in the solvent, while the uniformity, homogeneity and thickness of the printed pattern depend on the particle size.
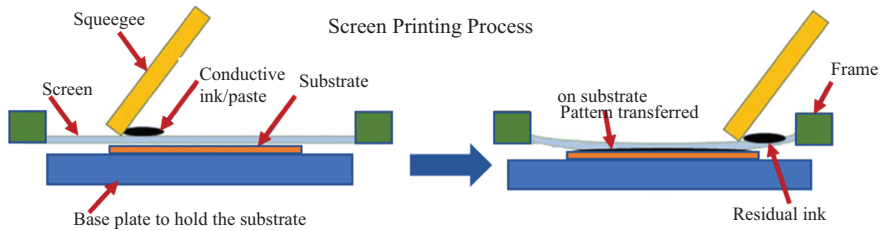
Figure 8.1 Screen printing process for flexible antennas and electronics

The screen is usually made with a fine net sheet coated with a photo emulsion with an engraved pattern designed to transfer the paste to the substrate placed under the screen frame. The complete screen printing process is presented in Figure 8.1. A reasonable level of prototyping accuracy can be achieved by a careful deploy-ment of the process. After transferring of the pattern, the next step involves the sintering of the printed surface. The desired level of conductivity is achieved after the curing and sintering of the printed prototype. Several methods have been developed for sintering by using heat, laser, ultraviolet (UV) beam exposure, etc. For instance, one method involves exposure of laser beam on the printed surface by using formic acid in a nitrogen atmosphere [36,37]. Belt furnace with formic acid dosing system is used where laser sintering is carried out on the FASTLAPS roll-fed prototype system [36,37].

8.2.2 Inkjet printing

Another additive manufacturing technique is inkjet printing which can successfully be used for an accurate fabrication of several printed circuits and antennas. For instance, the inkjet printing by using silver nanoparticle ink has been used on a flexible polydimethylsiloxane substrate in [38] and on a polyethylene terephthalate (PET) substrate in [39] for a wearable antenna fabrication. Recently, carbon-based compounds such as graphene enhanced nano-composite materials and carbon nanotubes (CNTs) have gained attention in the printable and flexible electronics to replace conductive metal inks. These biodegradable materials have many environment-friendly attributes, reduced cost as compared to metal-based inks and suitability to be used in antennas. For instance, a flexible and stretchable antenna on a stretchable single-walled CNTs/Lycra fabric is reported in [40]. Moreover, there are many stretchable conductive ink solutions compatible with the body-centric wearable antennas commercially available [41].

Advanced inkjet printers are designed with the drop-on-demand technology, where a piezo or thermo component is incorporated in the printer's printhead to generate pressurised pulses to control the ink discharge from the nozzle [35]. The entire inkjet printing process involves three essential stages: printing, sintering and characterisation as shown in Figure 8.2. Printing is performed by a set of nozzles integrated in the inkjet printer, conductive ink and an automated system, where the user controls the speed/jetting of ink, feature size and resolution, thickness of a
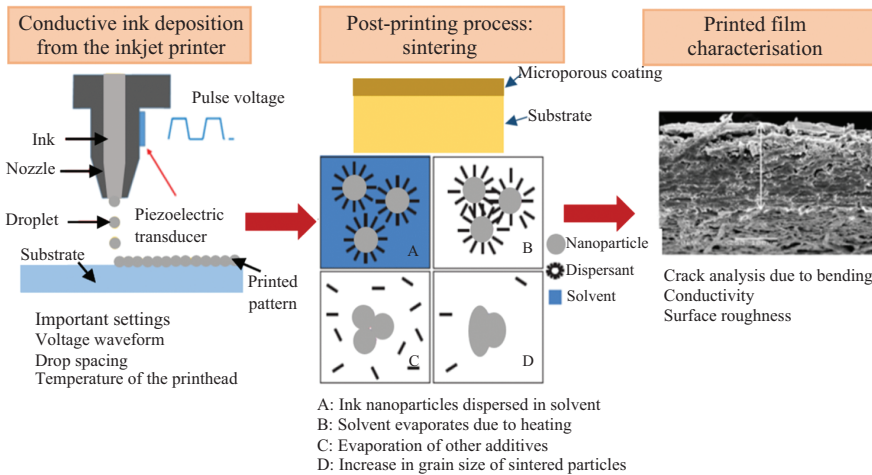
Figure 8.2   Inkjet printing process for antenna fabrication

single printed layer, drop spacing and thus the overall accuracy of the printed pattern. The next step is to sinter the printed pattern to improve the conductivity of the printed layer. In metal-based inks, the conductive particles are usually encap-sulated in a sheath of polymer to avoid oxidation due to solvent. Sintering involves breaking the sheath to release the encapsulated conductive nanoparticles. Laser sintering and heat sintering are two most used methods, where high-energy laser beam or heating at high temperature melts the polymer coating as well as the ink particles. The molten ink particles combine to form a continuous layer of metal. Laser printing is time efficient with a risk of defects if the intensity and time of exposure is not properly controlled. Some commercially available substrates are coated with a microporous layer that offers rapid drying of the ink and chemical sintering.

In general, the conductivity of a silver nanoparticle single layer is $0.3–0.7 \times 10^7$ S/m and can vary up to $0.4–2.5 \times 10^7$ S/m depending on the number of successive printing iterations, layer thickness, temperature, and curing and sintering durations [29,33]. Thicker layers provide better conductivity; however, thicker metal layers are more brittle and can be easily cracked by successive bending and folding in the case of flexible and wearable antennas. With an optimisation of these constraints, inkjet printing can be a reliable choice for wearable antennas.

8.2.3   Embroidery with conductive yarns

Embroidered textile-based antennas can be potentially used in a variety of wear-ables and can be easily integrated along with other woven electronic components as a part of daily garments. The fabrication of embroidered antennas is performed by using conductive threads and computer-aided embroidery machines to construct the antenna pattern on a textile substrate. Besides metal-based conductive threads,

many other polymer fibres with metallic coating have been introduced. These fibres comprise approximately 10-mm thick robust and flexible polymer core with a metallic coating of 2-mm thickness [42]. In order to achieve good surface uni-formity and high conductivity, fully automated embroidery machinery and high-density stitching are deployed. This method is suitable for the fabrication of a variety of textile-based embroidered wearable antennas, RF sensors and the asso-ciated electronic circuitries required for many body-centric applications such as medical monitoring, and RF identification and tracking. These fabric antennas have shown great potential for the 5G networks and beyond for future RF functionalised fashionable garments and body-worn communications due to excellent RF perfor-mance compatible to conventional rigid metallic antennas.

8.2.4 Woven and non-woven antennas

This method utilises the conductive sheet either sewed or glued on textile substrates. For instance, graphene sheets, copper and aluminium sheets, etc. are cut in a designed pattern by means of blade cutting or laser cutting and installed on the substrate with adhesives. Wearable antennas designed with metallic fabrics sewn on cotton, denim and other similar textiles have also been reported. Besides sewing the metallic sheet on a textile, the conductive fabric is often woven in a defined pattern by weaving. The common weaving techniques in this regard are basic plain weave which is strong and durable, and a rip stop weave that is effective to avoid tearing. Threads used for weaving are usually metal based such as silver, copper, nickel and tin in various combinations. The performance of these textiles-based antennas is usually char-acterised by repeated stress cycles that involve cold water washing, hot water soak-ing, outdoor drying, ironing, etc. and impact of these successive washing cycles on the conductivity, durability and adhesion and overall robustness of these antennas [43]. The use of graphene-based materials for flexible non-woven antennas is well known due to good conductivity and thin-film characteristics suitable of bending and folding. Graphene has an anisotropic two-dimensional (2D) shape and good proces-sability. A few layers assemble to form a flexible 'graphene paper' which offers good conductivity and can be deployed on various rigid and flexible substrates and even on textiles for antennas as demonstrated in recent works.

8.2.5 Vinyl cutters and plotters

Vinyl cutters and plotters have been widely used in several industries, for example within graphic design. Currently is being explored and applied for rapid prototyp-ing in label-type designs, mainly for UHF RFID tags. The method consists of shaping the antenna pattern on different films and substrates, employing cutter plotters to mechanically cut the structure according to the virtual design. Flexible adhesive copper sheets or other conductive films like graphene are used for this purpose, followed by either subtractive by removing the excesses or additive via transferring the final patterns on target soft substrates [44] (Figure 8.3).
This fabrication method is particularly suitable for cost-effective and time-saving antenna designs. No chemicals or heat is involved in this process, turning it
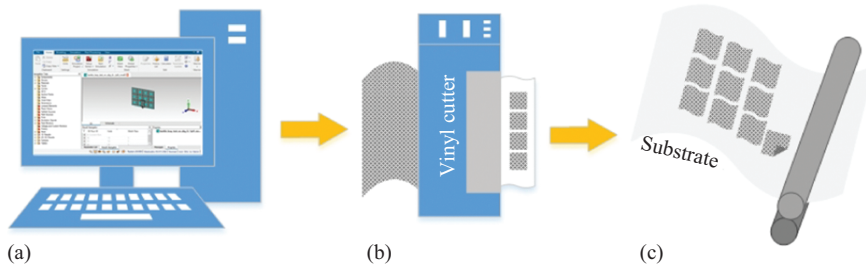
Figure 8.3   Flow chart of the procedure: (a) computational modelling; (b) cutting process; and (c) lamination on the substrate

into a suitable alternative for more complex techniques. These characteristics per-fectly match the requirements of soft electronics devices such as being planar, flexibility, stretchability, conformability, lightweight, as well as low cost. There is an ever-growing interest in this method for the digital manufacturing of flexible devices that is compatible with several materials such as sheets of metals [45] and even 2D materials like graphene [46].

Shape and size of the antenna will be constrained by the resolution of the cutting equipment. In the case of simple antenna patterns, 0.5-mm resolution is readily achievable, while for more complex shapes, recent studies claimed that 1 mm would be the smallest line completed [44]. These characteristics cope with the requirements for 5G antenna models in the frequency band of sub-6 GHz in [45] antennas operating around 2.45 GHz and in [46] from 3 to 9 GHz, have been manufactured following this approach. The improvement in the features of cutting equipment allows some plotters to for resolutions up to 24.5 mm [47], allowing us to reach the K band (i.e. 18–26.5 GHz). In Figure 8.4, some prototypes fabricated with this method are depicted even within at mm-wave frequencies Figure 8.4(g).

8.2.6   *Automated laser prototyping on flexible substrates*

Automated laser micromachining is one of the methods for flexible antenna fabri-cation [33]. Several rigid and flexible substrates laminated with copper and alu-minium are available that can be subjected to laser micromachining to etch out the designed pattern. The working principle of these laser-based machines is similar to basic printed circuit boards milling for electronic circuits and antennas, though these advanced machines use an extremely precise UV laser beam instead of metallic tools like mill/drill/router bits to remove metal in a specified pattern from the surface of the cladded flexible substrate. The laser beam prevents hazardous chemicals usage for etching, requires no masks or photolithographic patterning, time-efficient and holds minimum manufacturing cost. The laser probe operates in a contact-free environment and maintains an appropriate height above the substrate and thus can be easily used on delicate materials. These laser-milling machines are highly efficient in prototyping on both rigid and flexible substrates and provide fast and reliable fabrication with high accuracy.
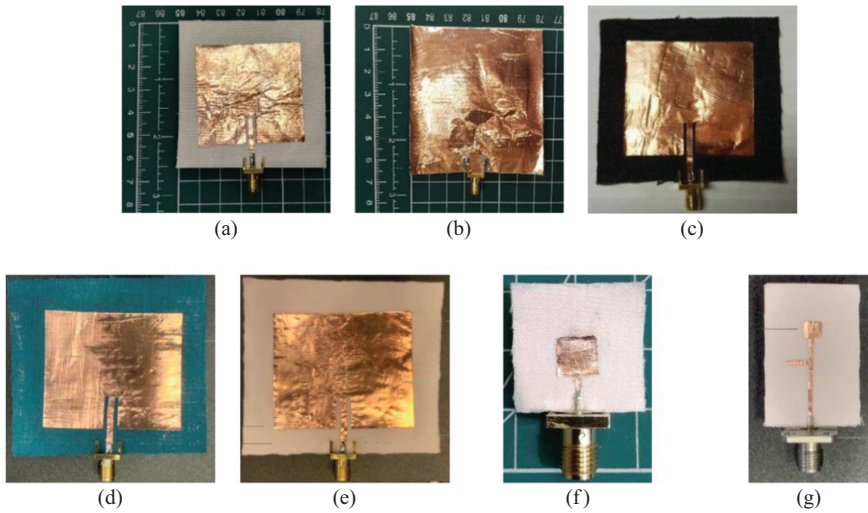
Figure 8.4   Photos of the antenna prototypes: (a) cotton top-view; (b) cotton bottom-view; (c) jeans; (d) viscose; (e) Lycra; (f) cotton at 9.45 GHz; and (g) cotton at 38 GHz [45]. Reproduced, with permission, from Isidoro Ibanez-Labiano, MDPI Materials; published by MDPI, 2020

8.3   Metrology techniques for wearable antennas

This section of the chapter describes measurement techniques of 5G wearable devices and antennas for on-body scenarios. Different set-ups are presented to evaluate the key features of wearable antennas.

For any type of antenna, measurement parameters such as scattering parameters (S-parameters), gain and radiation patterns can be evaluated within a far-field screened anechoic chamber using vector network analyser (VNA) to assess and analyse their basic radiation characteristics and features, where VNA is typical equipment used for classical antenna metrology. For the specific case of wearable antennas, measurements are often performed with either real human or human tissue equivalent phantom in order to take into account the impact of the human presence. The effect of the human body on the antenna's performance, as well as the consequences on human tissues as a result of absorbing RF energy, specific absorption rate (SAR). In reality, wearable systems often perform in a dynamic and constantly changing environment, where they should sustain their performance under physical changes for example bending and crumpling conditions. Environmental factors, including moisture and temperature variations, will modify the electromagnetic properties of the materials used in these wearable antennas, thus altering their radiation and link performance.

8.3.1   Phantom numerical and experimental evaluation

The effects of a numerical and physical phantom for different wearable antenna systems are presented later. Impedance bandwidth, efficiency and radiation pattern

are key characteristics of wearable antenna which are affected by the presence of the human body or phantoms [48]. The human body is inherently a lossy medium that in close proximity of an antenna has detuning effects and reduces its efficiency [49]. With a view to developing wearable devices for body-centric wireless appli-cations, it is crucial to characterise these effects. For these characterisations a part of a real human body, tissue-equivalent options are commonly used for numerical experimental analysis. This section describes such numerical and experimental human phantoms.

8.3.1.1 Electromagnetic characteristics of human tissues

For proper characterisation of the antenna's behaviour in the close proximity of the human body, the knowledge of dielectric properties of tissues is very important [48,49]. A consistent database of dielectric properties is really complex to achieve due to the properties of biological tissues that change with frequency, temperature, position and the type of tissue (water content) [49]. Figure 8.5 illustrates an example of the dielectric properties (relative permittivity e_r and conductivity s) for two types of human tissues that differ from water-content with fat having lower values than muscle. It can be seen that the dielectric properties are dependent on the frequency and water content.

Open databases of dielectric data, such as the one of the Institute for Applied Physics, are available for all tissues at single frequencies or for a single tissue in a full span between 10 Hz and 100 GHz [50]. Previous research studies have calcu-lated these characteristics: conductivity, s, relative permittivity, e_r, loss tangent, tand, and penetration depth for a number of different human body tissues at the Industrial Scientific Medical (ISM) band around 2.45 GHz [10]. In the case of
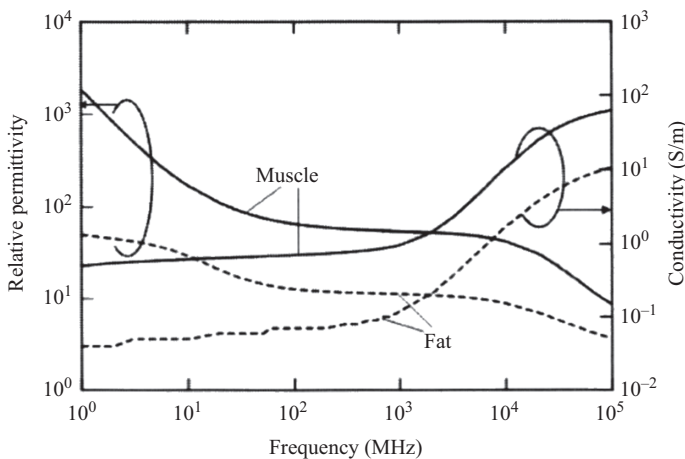

Figure 8.5   Dielectric properties of muscle and fat from 1 MHz to 100 GHz at 37°C [49]

Table 8.1   Dielectric properties of human body tissues at ISM Band – 2.45 GHz [50]

Tissue	ε_r	tanδ	σ (S/m)
Dry skin	38.007	0.28262	1.464
Fat	5.2801	0.14524	0.1045
Muscle	52.729	0.24194	1.7388

Table 8.2   Fully details of the seven models of the CST Voxel family [53]

Model	Age/Sex	Size (cm)	Weight (kg)	Resolution (mm)
Baby	8-week female	57	4.2	0.85×0.85×4.0
Child	7-year female	115	21.7	1.54×1.54×8.0
Donna	40-year female	176	79	1.875×1.875×10
Emma	26-year female	170	81	0.98×0.98×10
Gustav	38-year male	176	69	2.08×2.08×8.0
Laura	43-year female	163	51	1.875×1.875×7.0
Katja	43-year pregnant 24 weeks	163	62	1.775×1.775×4.84

body-worn devices, the main influential tissues are skin, fat and muscle date is depicted in Table 8.1.

8.3.1.2   Numerical phantoms

Theoretical homogeneous or layered flat phantoms are the most basic theoretical phantoms in simple shapes, which are used for running computational simulations and numerical analyses [46,51]. Thanks to the development of different technolo-gies such as X-ray, ultrasound, computed tomography and magnetic resonance imaging (MRI) [52] more complex models have been developed, Voxel models. Among commercial options, Computer Simulation Technology (CST) Studio Suite has a biological database that provides different solutions [53]. CST Voxel family with seven models represent seven persons of different gender, age and stature, Table 8.2. The three-dimensional computer-aided design models of the seven types of individuals are shown in Figure 8.6.

CST also provides a visible human model dataset with more layers and a specific anthropomorphic mannequin, which is for standardised certification pur-poses. Also, there are available different CTIA (Cellular Telecommunications and Internet Association) head and hand models to simulate different types of devices in several holding situations and again for certification purposes [53], see Figure 8.7.

8.3.1.3   Experimental phantoms

Usually, it is not recommended the use of a real human body for test campaigns due to the complexity of the set-up and health concerns [54]. For that purpose the vast range of experimental phantoms is employed, where they replicate a specific part of
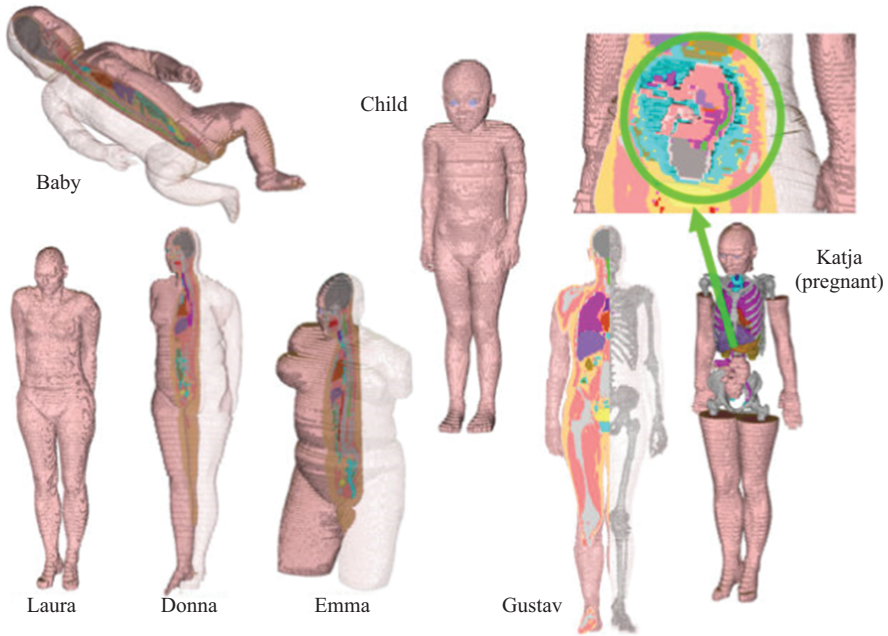
Figure 8.6   *CST Voxel family options: baby, child, Gustav, Laura, Katja, Donna and Emma* [53]
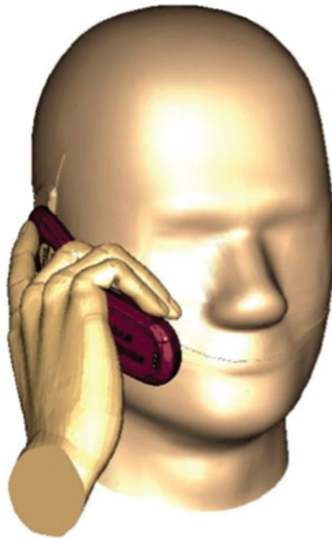

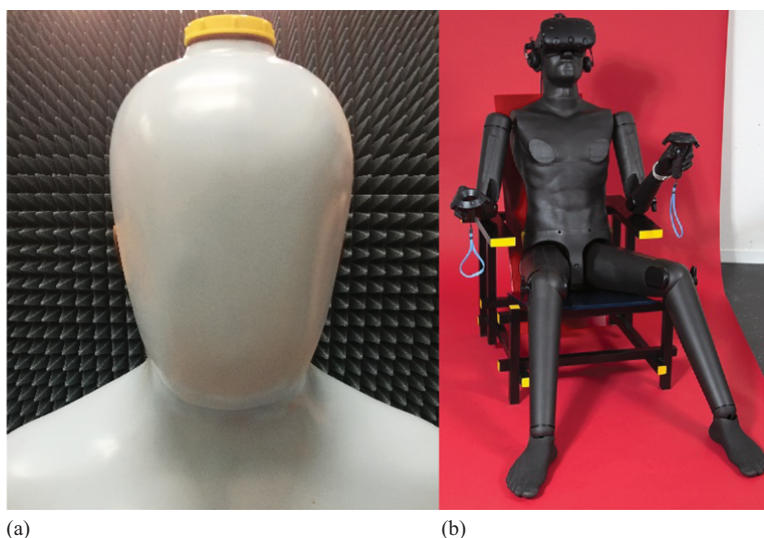Figure 8.7   *Phantom head representation holding a device* [53]

Figure 8.8   (a) Human bust mannequin and (b) SPEAG model [63]

the human anatomy or the whole body. One type of experimental phantoms are liquid ones [55,56], which usually are homogeneous but they cannot perform over a wide frequency range. They are typically containers filled with a mixture that replicates the dielectric properties of the human tissues that wanted to be mimic [46]. There is not a unique recipe, so different mixtures of solutions were proposed in the research literature [57–59]. In [46] a solution consisted of 79.7% of deionised water 0.25% of sodium chloride, 16% of Triton X-100 (polyethylene glycol monophenyl ether), 4% of diethylene glycol butyl ether (DGBE) and 0.05% of boric acid, was used to fill the phantom depicted in Figure 8.8(a). Other phantoms can be classed as a solid and can be cast into different sizes and shapes. They commonly used deionised water, sodium chloride, agar, sodium dehydroacetate and polyethylene powder TX-150 and TX-151, in various quantities for different solutions [60–62].

Their commercial solutions are available from the Swedish company SPEAG, one of the leaders regarding this area. One of its full model phantoms can be seen in Figure 8.8(b).

8.3.2   Mechanical durability of wearable devices

The fabrics are subjected to multi-directional stress and strain components; thus they behave non-linearly due to the mechanical interaction between human body and garment that depends on the garment style, garment space allowance, dynamic wearing and the posture of the human body [64]. Standard textile testing methods over current 2000 ISO, BS and ASTM standards are very well defined to assess mechanical, thermal and chemical stability of textile structures varying from fibres

to the final garments. Due to the lack of mechanical testing standard, specially narrated for wearable technologies, quite often the researchers have followed the methods proposed for the standard textiles. Thus, we expect a similar grade of durability and testing configuration in any textile-based electronic systems that might cause misinterpretation when the electronic integration has drastically influence the mechanical stability. Nevertheless, current textile testing standards include the following:

- Breaking Force and Elongation of Textile Fabrics (ASTM D5035-11:2019).
- Determination of the elasticity of fabrics, Multiaxial test (BS EN ISO 20932-2:2020).
- Determination of the elasticity of fabrics, Strip test (ISO 20932-1:2018).
- Determination of bending length and flexural rigidity of fabrics (BS 3356:1990).

    It is very challenging to do quantitative analysis; thus the appearance of

creases in the fabric after cleansing is assessed based on the test method BS ISO 7769:2009. Coupled with the electronic component, the textiles' behaviour when subjected to bending, folding and abrasion dominated the durability of e-textile, including smart fabric sensor or transducers, as stated in [65]. Hence, the antenna requires to match draping and haptic qualities of the textiles, especially if it would be worn on the body. References [66,67] have demonstrated that antenna under bending could widen the radiation pattern along the bending plane and amend the impedance matching. These results emphasised the necessity of user case predic-tions to adapt the communicating element along with the textiles and the integra-tion method, especially on body applications. How body medium impacted the absorption of EM radiation and the SAR distribution as a function of the antenna curvature sizes and different on-body locations and distances was pointed out in [68]. Hence, the bending rigidity of the antenna associated with the textile inte-gration method, including embroidery, printing and lamination, also have an impact on the antenna performance. Thus, stiff and robust embroidered antennas are less affected from the deviations in the bending curve.

    The researchers could tune the antenna operational frequency by predicting the bending and tensile performance of textiles, whereas the durability in terms of abrasion, especially in varying temperature and humidity conditions, is more unpredictable. Different test configurations described in the following ASTM D4970/D4970M – 16e3Standard Test Method for Pilling Resistance and Other Related Surface Changes of Textile Fabrics: Martindale Tester, ASTM D3885 –07a(2019) Standard Test Method for Abrasion Resistance of Textile Fabrics (Flexing and Abrasion Method) and ASTM D4157 – 13(2017) Standard Test Method for Abrasion Resistance of Textile Fabrics (Oscillatory Cylinder Method), and other abrasion standards can be followed to monitor the changes in the post-and pre-antenna performances. A similar approach was conducted in [69] to understand the effect of abrasion on the surface conductivity of nickel–copper yarn-coated nylon ripstop and silver yarn-coated cotton/polyester jersey knit and reported the damage on the surface associated with the increased resistivity.

8.3.3   Specific absorption rate

SAR is a measure widely used to verify how much energy is absorbed by a human body when this is exposed to an electromagnetic field of transmitters operating at frequencies from 300 kHz to 100 GHz. Mobile phone operations and MRI scans are two of the most common areas where this measure is required. It is commonly defined as the power absorbed per mass of human tissue, units of watts per kilo-gram (W/kg):

$$SAR = \frac{1}{V} \int_{Sample} \frac{\sigma(\boldsymbol{r})|\boldsymbol{E}(\boldsymbol{r})|^2}{\rho(\boldsymbol{r})}\, d\boldsymbol{r},$$

where s is the electrical conductivity, $\boldsymbol{E}$ is the electric field, r is the sample density and V its volume.

The SAR testing is normally carried out using electric field probes [70], usually dipole antennas, submerged in a phantom that mimics the human tissue to be analysed. Several factors have to be taken into account, such as part of the body that is exposed to RF energy plus its shape, and intended position of RF source. Tests must replicate as accurate as possible the operational environment of the wearable system.

In some cases, temperature probes are placed to quantify temperature increase. Although temperature distributions do not always correlate well with SAR dis-tributions, and that regulatory thresholds on local temperature values may not be surpassed as readily as those on local SAR [71].

Numerous measurement standards and directions, such as the IEC 62209-1 (head) and the IEC 62209-2 (body-worn, separation distance of up to 25 mm can apply), have been released to cover the standardisation of these types of measurements. IEEE STD 1528 IEEE is a recommended practice for measurements and computations with respect to human exposure on electromagnetic fields, from 100 kHz to 300 GHz. The Federal Communications Commission (FCC) proposes the FCC OET 65 Supplement C to evaluate the compliance of human exposure to RF energy. Most of the guidelines are cover in the International Commission on Non-Ionizing Radiation Protection (ICNIRP) 2020 Guidelines [72]. ICNIRP has been recommended by the International Telecommunication Union and World Health Organization.

8.3.4   Durability and washing tests

Sufficient knowledge must be possessed about the performance of the commu-nication element under deformation and chemical agitation to strategically plan-ning out the positioning and the antenna design itself. Textiles especially worn on the body are prone to abrasion and cyclic deformation that is associated with the dynamic wearing and environmental conditions and later care, including launder-ing. Coupled with the anisotropic textiles, it could be challenging to predict the durability of the communicating element. Reference [69] investigated the effects of pilling, wrinkling, abrasion and laundering of e-textiles by examining the surface resistivity performance from both direct current and radiofrequency perspective.

Proposed micro-strip patch antenna design made of copper yarn-coated nylon ripstop on durable denim fabric was tested by following ASTM D3512 to reveal the effect of pilling on reflection coefficient, S_{11}, and realised gain. The results demonstrated that the gain dropped almost 20 dB due to severe damage on the conductive coating of the fabric. However, wrinkling did not exhibit such a dra-matic effect on the conductivity. As revealed by [73], printed conductive tags suffered more than conductive coated fabrics due to the inherent discontinuity along the surface when subjected to abrasion and pilling. The protective measures against environmental effects that included preshrinking of new fabrics to prevent the resonance shift of fabricated antennas over time and textile protective layers to shield water absorption and salt contamination related to the human bodily fluids and the harsh environments and abrasion were discussed in [74]. Particularly in conductive fabrics and inks made of different metals and their derivatives, the antenna performances were drastically influenced by the environmental conditions such as humidity, water/salt absorption and temperature due to oxidation and changes in electrical conductivity. They emphasised the importance of the chemical nature of water repellent coatings and additional security measures about how strong salt solution was capable of dissolving the protective barrier and reached the conductive metallic layer. At cryo temperatures, it was also reported that the ice significantly changed the antenna impedance matching [75]. Thus, we are expect-ing the same material failures associated with both printed and coated nanomaterial based wearable antennas that might become vulnerable due to external factors, including the temperature changes and humidity.

Despite all the recent efforts in the literature [76,77], from the perspectives of electronics, 'care' of antenna systems when placed on the body is still very intri-guing and also highlights the practical limitations of antenna design. Lacking e-textile durability standards that include laundering or pilling makes the design impractical to compare different textile-based systems either made of conductive inks, yarns or fabrics. Nevertheless, we had clues how various textile forms ensured washing durability. On the first attempts on revealing the durability of laundering, Scarpello *et al.* [78] imposed a breathable thermoplastic polyurethane coating to protect the screen printed microstrip inset-fed patch antenna from water absorption and corrosion. They introduced the protective layer by ironing and explored the two competing parameters, reduced conductivity due to melted polymer and diminished roughness that had a positive contribution by reducing the surface resistivity. It is evident that applied thermal post-processes, including the ironing, led to more compact structures, especially working with conductive ink-based surfaces [78]. Either using metal-deposited fabrics or conductive inks, the mainstream approach is to apply superhydrophobic coatings to inhibit water absorption even after mul-tiple wash cycles [79]. In particular, nanomaterial-based inks or screen-printed surfaces are susceptible to water migration and contamination through the cracks, where the pores are unavoidable due to the textile manufacturing method. Thus, washing durability of the textile antenna is strongly dependent on the physical and chemical absorption mechanism and surface quality, including cracks and uni-formity. Even it is not inevitable, the antenna performance could be predicted to

some extent. For instance, Carla *et al.* [80] revealed how increasing moisture could increase the permittivity and loss tangent of the textile material that led to a decrease in antenna efficiency by changing the resonance frequency. In [46] was reported the washing durability of graphene-based ultra-wideband (UWB) textile antennas by following the standard protocol in BS EN ISO 6330.

Reference [74] pointed out the uncertainties in the antenna modelling asso-ciated with the textile substrates and suggested the following protocol (i) modelling of conductive fabrics/patches or surfaces using impedance models to predict non-ideal conductivity, (ii) understanding the changes in permittivity either by washing or other external factors that could change the air gaps or the volume of air trapped in textile structure, (iii) assembly of the wearable antenna system, for instance attaching conductive layers to the textile. These points highlighted the hetero-geneous medium along with the challenges in standardisation of e-textiles, including the antennas. Nevertheless, the current efforts on the standardisation of wearable electronic devices and technologies include a broad scope of testing methods such as BS EN IEC 63203-201-1: measurement methods for basic prop-erties of conductive yarns, BS EN IEC 63203-201-2: measurement methods for basic properties of conductive fabric and insulation materials, BS EN IEC 63203-201-3: determination of electrical resistance of conductive textiles under simulated microclimate, BS EN 63203-204-1: washable durability test method for leisure and sportswear e-textile system and a standardisation in the terminology, BS EN 63203-101-1. Wearable electronic devices and technologies. Part 101-1. Terminology. 'Wearable electronics' coupled with the textiles is a still-developing field that has the potential to evolve more mature systems and technologies as in PD IEC/TR 62899-250:2016 Printed electronics. Material technologies required in printed electronics for wearable smart devices. More remarkably, when planned out to position the nanomaterial-based antenna systems either on the body or in the proximity of the human, it is highly recommended to follow the guidance on per-forming tests to simulate nanoparticle release, PD CEN/TR 17222:2019S: textile products and nanotechnologies: skin exposure and addressed the prospective safety issues for wearable applications.

8.3.5 Environmental factors (humidity and thermal tests)

Moisture and temperature are the two most common environmental factors to be analysed within wearable systems with respect to their impact on antenna's per-formance. The effect of these two factors can be measured following two different approaches – first by characterising the variations of the parameter itself, and second by measuring the alteration of the antenna's performance due to the change of the parameter – in both cases under a controlled environment.

Regarding the first case, dedicated methods previously described in the lit-erature [81–83] are used to measure specific constitutive material parameters of the antenna, such as conductivity, s, permeability, m, and permittivity, e, under varia-tion of the environmental conditions. In the case of electrical conductivity, the standard procedure is to use a multimeter or a more precise instrument like a

four-probe set-up and considering the geometry of sample [81]. For material characterisation in terms of dielectric properties, several methods are available, from microwave theory, they can be split up into two complementary types: non-resonant and resonant [82,83]. Within these two kinds, there are several sub-categories with their respective specific tools and apparatus. Each method has its pros and cons, so a trade-off is necessary for each case, but a general rule is to use non-resonant methods for wideband measurements and resonant ones for concrete frequencies. The second mechanism is based on measuring the changes of the antenna performances under certain environmental conditions, seeing the indirect impact of the changes from the parameters previously mentioned.

For instance, relative humidity (RH) has an impact on the antenna's behaviour by increasing its dimensions (substrate's thickness) [84], as well as rising the dielectric constant value due to moisture absorption [85]. These characteristics have motivated several research studies regarding the use of antennas as humidity sensors, mainly focusing on wearable technology [86,87]. In the case of tempera-ture, generally, conductivity increases as materials get colder, as there is less atomic activity bouncing and the electrons can move more freely. It will affect the e_r as well and consequently will influence the resonant frequency (f_r) of the device. Rising temperature in solid materials permits the dipoles of the molecules more free movement (like the case of electrons), conveying to an increase in the per-mittivity value. In cases with less restrains, such as liquids and gasses, this has an adverse effect [45].

For all cases, environmental factors can be taken into consideration during numerical analysis by performing parameters sweep in commercially available full-wave electromagnetic simulation software (CST Studio Suite). Other programs such as COMSOL Multiphysics can run multi-physics analysis, where an envir-onmental factor coefficient can be inserted. For the purpose of test campaigns, several commercial solutions of environmental chambers, also known as climatic or climate chambers, are available.

These chambers are capable of artificially replicating different environmental conditions for a device under test (DUT). This environmental test equipment is able to accelerate the changes in the conditions or extreme situations in a controlled manner recording all the data. Several conditions can be manipulated such as temperature, moisture, UV and/or vacuum. Figure 8.9 depicts the diagram of a set-up to measure *S*-parameters of an antenna, where the DUT is placed inside the climatic chamber and then connected to the analysing equipment (in this case a VNA), and Figure 8.9(b) shows one of the commercial options. Depending of the test to be carried out, more bespoke solutions can be set [45].

8.4   Wearable antennas for 5G and beyond

8.4.1   *Ultra-wideband frequency-reconfigurable antenna*

A UWB-wearable reconfigurable antenna is presented in this section. The proposed configuration combines frequency and pattern reconfiguration on textile materials
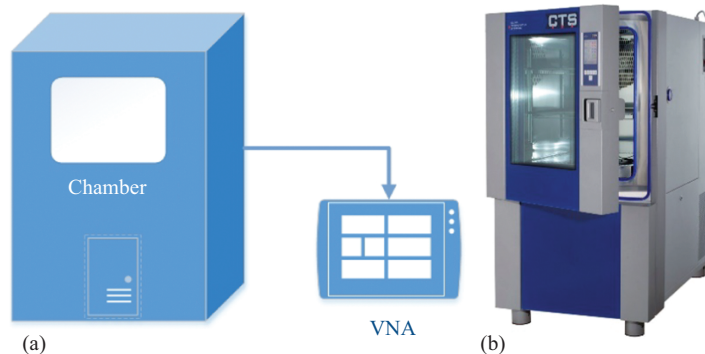
*Figure 8.9   (a) Diagram of a thermal set-up and (b) CTS commercial ambient
        chamber [88]*

and suitable for integration as a part of a military uniform or any clothing. Two different methods have been adopted to fabricate the patch and ground on a textile substrate. One method is conductive thread embroidery that was to fabricate the antenna on fabrics such as leather and cotton as a substrate. However, in the second method, a thin copper sheet was cut by using a laser cutter and mounted on the substrate. Commercial self-adhesive copper textile sheets were used.

The geometry of the antenna is based on the design proposed in [89,90]. Figure 8.10 presents the design proposed in [89,90], though the antenna dimensions have been optimised according to the dielectric properties of the textile substrates [91]. The proposed antenna offers both frequency and pattern reconfiguration, where the stubs length from the front part reconfigured the frequency while pattern reconfiguration was done by the two semi-elliptical stubs located on the back side. Connecting the ground plane with any of the stubs changes the radiation pattern of the antenna. The connected stub acts as a reflector and shifts the beam towards the opposite direction. As depicted in Figure 8.10, by using these two stubs, the radiation pattern can be reconfigured to the þx-axis and −x-axis of the antenna geometry. The dimensions of the proposed textile antenna are tabulated in Table 8.3 [91].

The 50-W matched feedline is designed for all the proposed configurations. In the first configuration, no stub was connected to the feedline and the antenna was tuned in UWB configuration that covers approximately 3–8 GHz. The proposed design in [89–91] reconfigured the frequency in six different bands. Table 8.3 depicts the designed dimensions and Table 8.4 presents the obtained bandwidth with respect to the proposed switch configuration as shown in Figure 8.10.

The simulation was done in CST Studio Suite. The pattern reconfiguration is performed with the semi-elliptical stubs included in the ground geometry. Each stub acts like a reflector to switch the radiation beam of the antenna to the opposite side when connected to the ground. Therefore, three modes are generated: (i) Mode 0: when no stub attached with the ground plane; (ii) Mode 1: the switch on left side
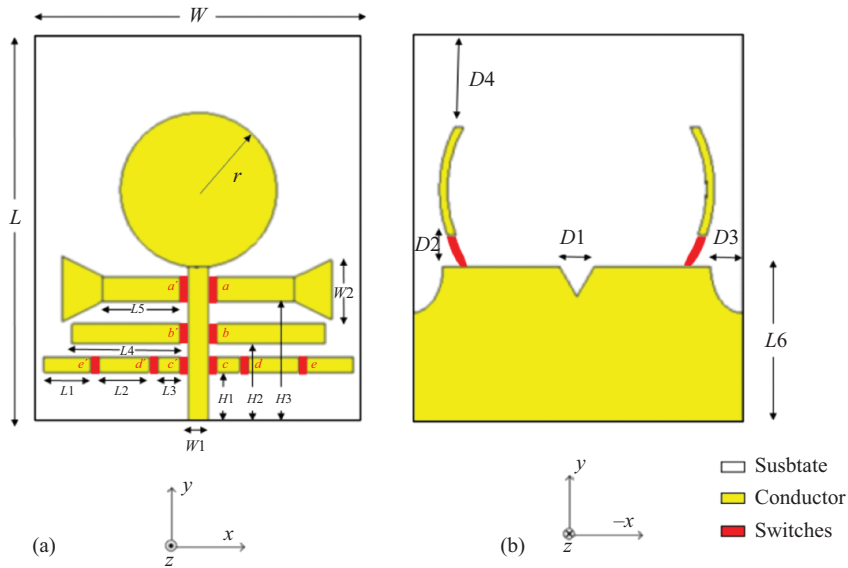
Figure 8.10   The proposed multi-mode reconfigurable ultra-wideband antenna: (a) front view, (b) back view [91]. Reproduced, with permission, from Syeda Fizzah Jilani, EuCAP 2016; published by IEEE, 2020

Table 8.3   Dimensions of the proposed textile-based antenna

Dimensions	mm	Dimensions	mm
Radius of the patch, r	10	Ground length, $L6$	20
Width of the antenna, W	42	First distance from bottom edge, $H1$	6.3
Width of the patch, $W1$	3	Second distance from bottom edge, $H2$	10
Stub width, $W2$	8	Third distance from bottom edge, $H3$	15
Length of the antenna, L	8	Length of V-cut, $D1$	4.5
First stub length, $L1$	8	Distance of reflector, $D2$	4
Second stub length, $L2$	4	Distance of reflector, $D3$	4
Third stub length, $L3$	18	Distance, $D4$	8
Fourth stub length, $L4$	10	Substrate thickness	1
Fifth stub length, $L5$	10	Conductive path thickness	0.08

is connected (ON) and the switch on right side is OFF (not connected); and (iii) Mode 2: the switch on left side is OFF and the switch on right side is ON, which results in ±90° beam shift from broadside to the þx-axis and −x-axis.

Five textile-based antenna prototypes were fabricated and the effect of mate-rials on the antenna performance was investigated. In first two antennas, the con-ductive sewing thread embroidery using an embroidering machine was employed as shown in Figure 8.11. Next three antennas were fabricated by using VLS6.60 laser cutter to cut the metallic pattern from thin conductive textile sheets

Table 8.4   Switch configuration and respective applications [91]

Switch configuration	Switches ON	Bands (GHz)	Application
Ultra-wideband	None	3–8	Cognitive radio
1	*c, c'*	2.4	ISM (industrial, scientific and medical) [10]
2	*c, c', d, e*	3.2–4.2	Wi-Max (Worldwide Interoperability for Microwave Access) [11]
3	*a, a'*	4.1–5.4	Some fixed mobile and satellites applications, Wi-Fi (Band A)
4	All	5	Wi-Fi
5	*b, b'*	6.5–7.5	Some fixed mobile and satellites applications
6	*c, c', d*	2.4; 5	ISM and Wi-Fi

(a)   (b)

Figure 8.11   Front and back view of two embroidered: (a) antenna on leather and (b) antenna on cotton [91]. Reproduced, with permission, from Syeda Fizzah Jilani, EuCAP 2016; published by IEEE, 2020

Table 8.5   Details of the fabricated prototypes of antennas

[91]

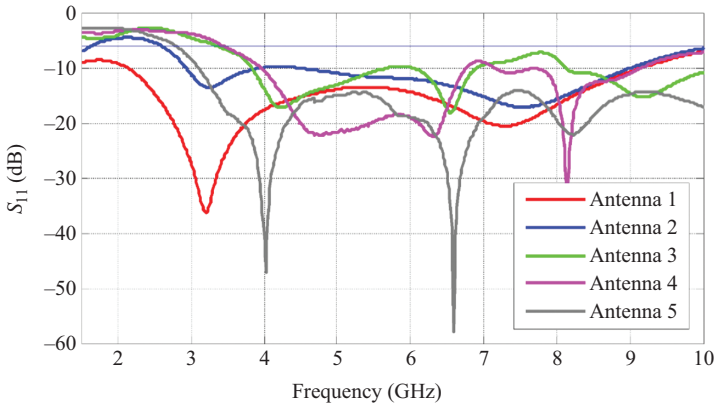| Fabricated antenna	Substrate used	Material used
Antenna 1	Cotton denim (ε_r=1.2)	Conductive sewing thread
Antenna 2	Cotton calico (ε_r=1.2)	Conductive sewing thread
Antenna 3	Cotton denim	Copper fabric
Antenna 4	Cotton calico	Copper fabric
Antenna 5	Leather (ε_r=2.3)	Copper fabric

Figure 8.12   Measured S_{11} plots of the proposed textile-based antennas at the ultra-wideband configuration [91]. Reproduced, with permission, from Syeda Fizzah Jilani, EuCAP 2016; published by IEEE, 2020

and sticking it to the fabric with conductive glue. The fabrication details of the antennas are provided in Table 8.5. The conductive epoxy is used to connect the antenna stubs by creating a short circuit as an ideal switch.

The reflection coefficients, S_{11}, of the proposed antennas are measured by using a VNA. The measured S_{11} for antennas 1–5 is shown in Figure 8.12 in UWB configuration.

Based on the testing of the fabricated antenna, Table 8.6 was developed to tabulate the obtained corresponding active bands. It is observed that antennas 1, 2 and 5 cover maximum number of bands in different switch configurations.

8.4.2   Millimetre-wave flexible antenna design

and metrology

In this work, a flexible beam scanning mm-wave array has been introduced. The design methodology of the proposed antenna has been derived from the series arrays; widely reported as fixed-beam arrays, frequency scanning and leaky-wave antennas (LWAs) [92]. The collinear principle, by the Franklin's collinear arrays of patch antennas demonstrates that by using non-radiating quarter-wave stubs for

Table 8.6 The operating bands obtained from the fabricated antennas in different switch configurations [91]

Antenna	Operating bands at different switch configurations
Antenna 1	Ultra-wideband, 3.2–4.2, 4.2–5.4, 6.5–7.5 GHz
Antenna 2	Ultra-wideband, 3.2–4.2, 4.2–5.4, 6.5–7.5 GHz
Antenna 3	Ultra-wideband, 2.4 GHz
Antenna 4	Ultra-wideband, 4.2–5.4 GHz
Antenna 5	Ultra-wideband, 2.4, 4.2–5.4, 6.5–7.5 GHz

180° phase shift in a series of patch antennas, the original out-phase current dis-tribution can be converted into an in-phased current on each collinear segment that provides one major radiating beam in a broadside direction [93–95]. Several modifications have been reported in Franklin arrays concept in order to achieve high-gain characteristics [96,97]. Besides, these arrays typically offer narrow bandwidth, as the design geometry is particularly based on the quarter-wavelength of the selected centre/resonant frequency. This work improved this limitation and presented a flexible and wideband LWA with frequency scanning. The proposed flexible antenna array retains the high gain of conventional Franklin array with the additional features of beam steering over a wide bandwidth.

In typical Franklin array assembly, each unit cell consists of a patch and a transmission line or a stub designed with the radiating length of quarter-wavelength (l/4) (i.e. $f = c/l$, where $f =$ resonant frequency, $c =$ speed of light and $l =$ wavelength). These unit cells are repeated to construct a linear array. In this work, array bandwidth is improved by changing the design lengths of the geometry with respect to the lower and upper cut-off frequencies of the intended bandwidth. Thus, the patch length is $l_L/4$ and stub length is $l_U/4$ in order to generate two individual resonant bands at lower cut-off (f_L) and upper cut-off frequency (f_U). In addition, the operating bandwidth between the two designed resonances is adjusted by means of parametric analysis of the patch width, stub width and the gap between the folded stubs [16].

The optimised dimensions of antenna design shown in Figure 8.13 are provided in Table 8.7. Simulation of the proposed mm-wave antenna array is carried out using the CST Microwave Studio software. The six-element array is designed on the PET substrate of $12 \times 28.2 \times 0.4$ mm^3 with a continuous metallic ground at the bottom. Height of substrate (h) is 0.4 mm for good return loss magnitudes while retaining the desired flexibility of the substrate. Designed array is fabricated on a surface-treated PET film ($e_r = 3.2$, $\tan\delta = 0.022$ at 10 GHz) from Mitsubishi Paper Mills with silver nanoparticle ink by inkjet printing process. The drop-spacing of 15 mm (i.e. 1,693.33 dpi), firing voltage of 15 V and jetting frequency of 5 kHz have been set on the Dimatix Material Printer. Three PET sheets each of height of 135 ± 12 mm are bonded together by means of double-sided tape to attain $h = 0.4$ mm. The nanoparticle silver ink was used for printing and a conductive layer with a thickness of 0.5 mm was deposited on a PET substrate with a pattern resolution of ± 20 mm. Post-printing drying, curing and sintering processes were performed to improve the conductivity of
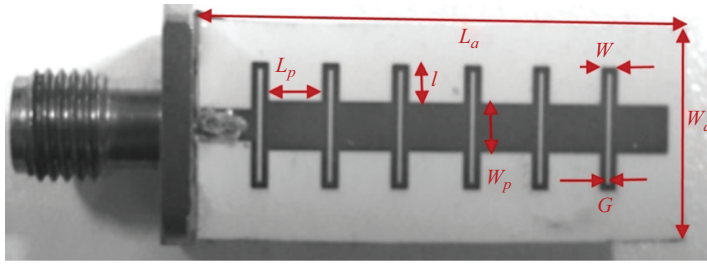
Figure 8.13   Proposed mm-wave leaky-wave antenna (LWA) mm-wave frequency-scanning array fabricated prototype [16]. Reproduced, with permission, from Syeda Fizzah Jilani, IEEE AP-S Symposium; published by IEEE, 2020

Table 8.7   Optimised dimensions of antenna design

Design parameters	mm	Design parameters	mm
Patch length, $L_p=\lambda_L/4$, $f_L=24$ GHz, $\lambda_L=12.5$ mm	3.1	Length of the folded stub, $2l+w=2\times(\lambda_U/4)$, $f_U=30$ GHz, $\lambda_U=10$ mm	5.2
Patch width, W_p	2.7	Gap, G	0.3
Length of the stub, $l\approx\lambda_U/4$	2.15	Feed width, w	0.9

the printed layer. The selected PET substrates are coated with a chemically active microporous adhesive that provides rapid drying and chemical sintering of the ink. This chemical method avoids a need of laser exposure or high-temperature sintering treatments that may cause bending, shrinking, decolourisation or melting, if the exposure energy or temperature is not appropriately handled.

The S_{11} plot of Figure 8.14 shows a good agreement between the measured and simulated results, hence validating the proposed findings of the designed antenna array. Measurements have shown that a bandwidth of 24.6–30 GHz has been achieved. Figure 8.15 depicts that the directive beam scans the spherical quadrant from the broadside to end-fire direction, as the frequency sweeps from 24.6 to 30 GHz. Figure 8.16 shows the numerically evaluated realised gain and efficiency vs. frequency of proposed array. The peak gain is 8.3 dBi at 28 GHz, and efficiency is approximately 60% in the overall operating range of the antenna. This flexible antenna is a good contribution in the development of the body-centric devices for future medical, security and many other communication applications because of its distinctive features.

8.4.3   On-body measurements on wearable antennas

In [46] a graphene textile-based UWB antenna was designed to cover a wide bandwidth ranging from 3 to 9 GHz. In this study, a numerical and experimental
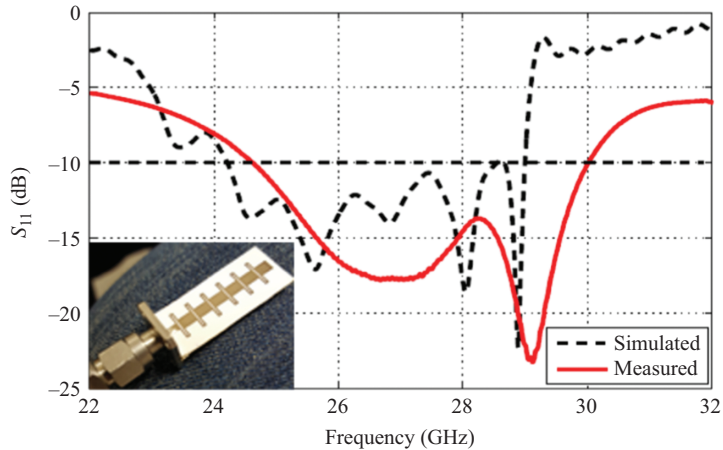
Figure 8.14   Simulated and measured S_{11} plots of proposed mm-wave frequency-scanning array [16]. Reproduced, with permission, from Syeda Fizzah Jilani, IEEE AP-S Symposium; published by IEEE, 2020

analysis of the antenna performance under the presence of a phantom model of human body parts was carried out.

For the simulations, a block of four layers in total, 44-mm thick (the thickness of body skin, fat and muscle layers were 1, 3 and 40 mm, respectively), was used. The electromagnetic properties employed of the different tissues – dielectric con-stant, e_r, loss tangent, tand, conductivity, s, and resistivity, r – are listed in Table 8.1 [50,98]. A 2D representation of the model is depicted in Figure 8.17(c). In order to look into the effects of the human body experimentally, a torso phantom loaded with a liquid to replicate human tissues was used. The solution selected is explained in Section 8.3.1.3; 79.7% of deionised water, 0.25% of sodium chloride, 16% of Triton X-100, 4% of DGBE and 0.05% of boric acid, which stuffed the torso phantom shown in Figure 8.17(b).

A test campaign was carried out at the Antenna Measurement Laboratory at Queen Mary University of London [99] with the aim to evaluate the performance of the antenna in the vicinity of a human phantom. For measuring the return losses, a VNA, PNA-L Agilent N5230C, was connected to the antenna under test (AUT). This set-up was calibrated with a standard electronic calibration kit to the end of the coaxial cable to have the same initial reference for all the measure-ments, for reproducibility purposes. For calculating the radiation properties of electromagnetic compatibility (EMC)-screened anechoic chamber equipped with two open boundary quad-ridge horn antennas operating from 400 MHz to 6 GHz (ETS-Lindgren 3164-06) and from 0.8 to 12 GHz (Satimo QH800), granting measurements in both vertical and horizontal linear polarisations were used, Figure 8.17(a).
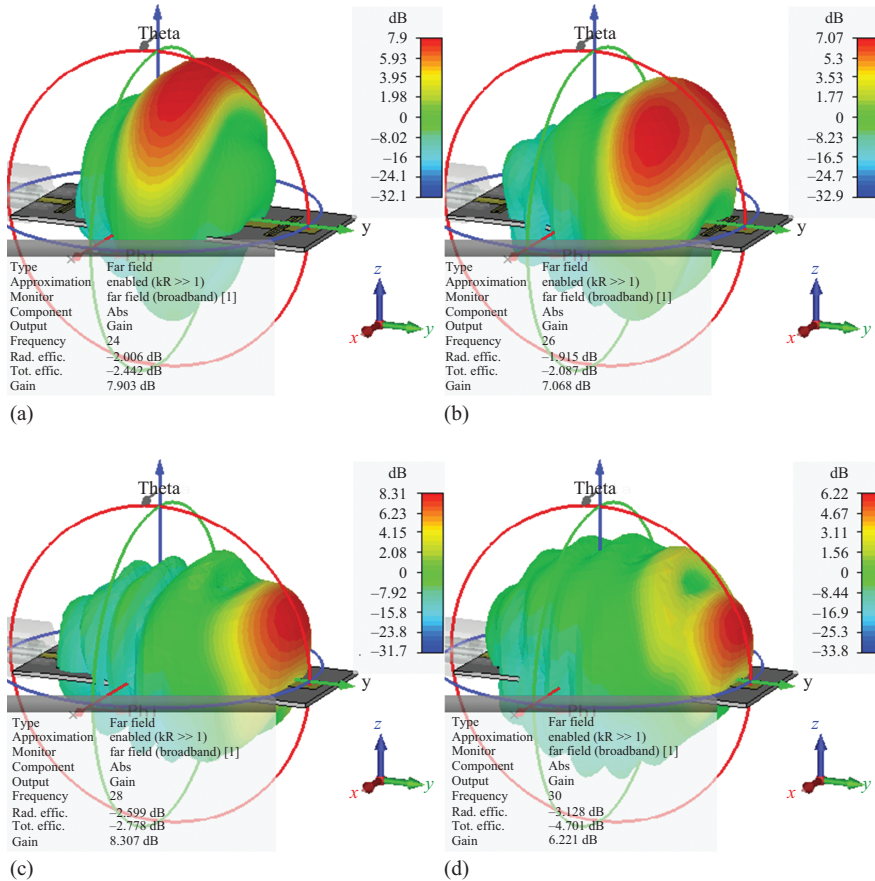
Figure 8.15 *The simulated EM radiation patterns of proposed mm-wave frequency-scanning array: (a) at 24 GHz; (b) at 26 GHz; (c) at 28 GHz; (d) at 30 GHz [16]. Reproduced, with permission, from Syeda Fizzah Jilani, IEEE AP-S Symposium; published by IEEE, 2020*

Figure 8.18 shows that the simulated on-body scenario exhibited a return loss of less than 10 dB in a wider range (2–12 GHz) in comparison with the off-body case (3–11.5 GHz). The slight frequency detuning and this increase in bandwidth could be due to the dissipative nature of the medium, the human body. It can be seen that the correlation between simulated and measured results, thus validating the model used.

Figure 8.19(a)–(f) presents the measured and simulated radiation patterns of the AUT for the on-body scenario, for frequencies: 3, 5 and 7 GHz. As well as for the return losses, the far-field measurement results agreed significantly with the simulated ones. However, due to the absence of a background plane that shields the antenna from the body, the antenna radiation properties were being affected.
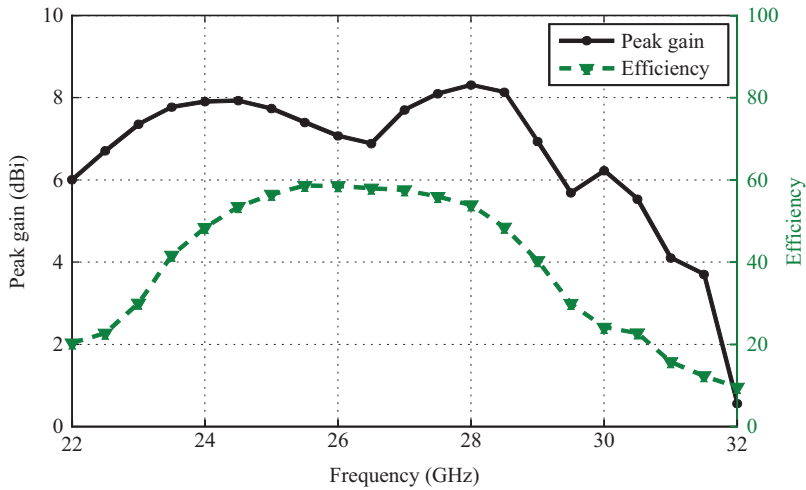
Figure 8.16   Peak realised gain and efficiency vs. frequency of proposed mm-wave frequency-scanning array [16]. Reproduced, with permission, from Syeda Fizzah Jilani, IEEE AP-S Symposium; published by IEEE, 2020
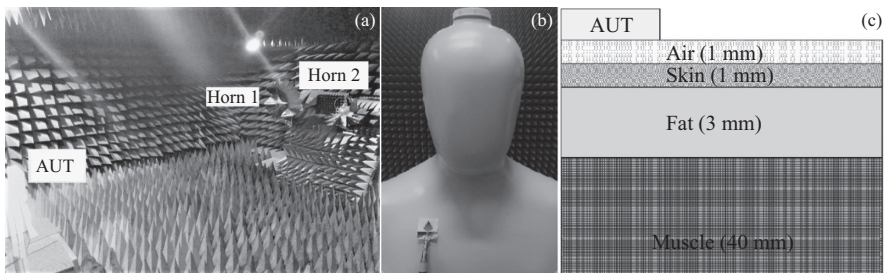

Figure 8.17   (a) EMC chamber set-up used in this study, (b) an image showing an AUT on a phantom and (c) four-layer phantom model used for on-body simulations [46]. Reproduced, with permission, from IIL, Applied Materials Today; published by Elsevier, 2020

The front-to-back ratio (*F/B* ratio) rises as the phantom absorbed the reflected waves that accompanied radiation at the front furthermore, which can be noticed that the experimental phantom absorbed more energy than the numerical model. This deviation in the expected behaviour is due to the complexity of exactly replicating the human model with all its variables.
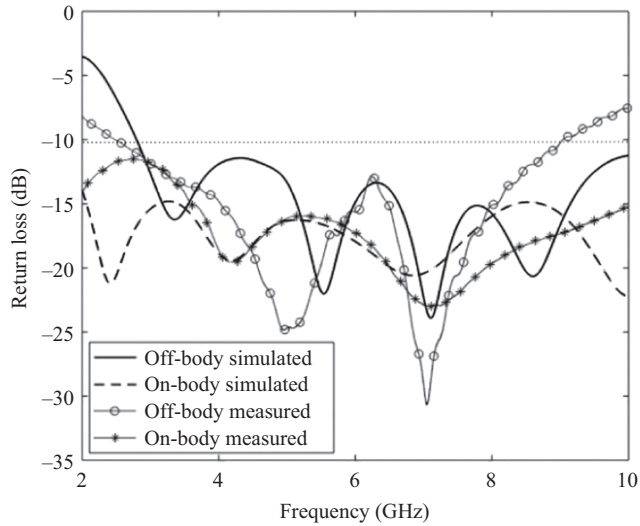
Figure 8.18   Simulated vs. measured S_{11} of graphene-based antennas in off- and on-body settings [46]. Reproduced, with permission, from IIL, Applied Materials Today; published by Elsevier, 2020

8.5 Conclusions

With the growing interest in 5G wearable antennas, especially for wearable body area networks applications, novel materials and fabrication techniques are being investigated and they were discussed in this chapter. Different methods such as screen printing, inkjet printing, embroidery, used conductive yarns and fabrics, and cutters were explained and evaluated. Each manufacturing technique was analysed in detail considering materials that can be used and the properties obtained for the antennas fabricated by that process. Every method has been supported by examples and references to facilitate the comparison between techniques and to highlight their advantages and features.

Current developments in the field focus on improving the efficiency and pre-cision of the manufacturing techniques, employing new flexible materials as a substrate, orientated towards higher frequency bands like the mm-wave band that demands high accuracy and precision. For this purpose, additive manufacturing techniques such as inkjet printing stands out and besides reduce the waste of material. Although in certain cases post-processing is required and that proposes a challenge for some materials like textiles. Novel conductive materials such as yarns or cloths and carbon-based ones like graphene, with a high conductivity, can be applied for the new fabrication and printing techniques. Graphene and other carbon-based solutions are promising alternatives to conventional metallic materi-als on the market, possess various properties, including electrical and thermal conductivity, optical transmittance and high strength/stiffness.
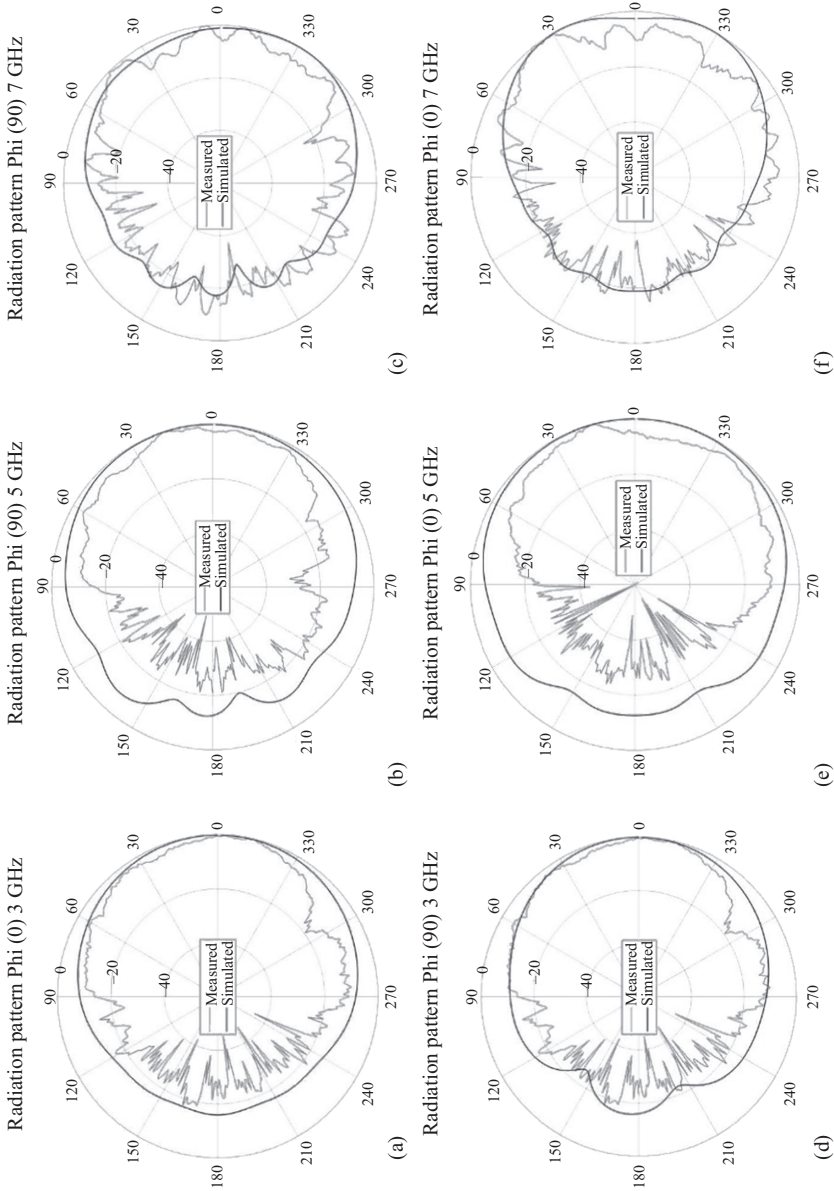
Figure 8.19 Measured vs. simulated radiation pattern of the proposed graphene-based antenna on the phantom at: E-plane cut, at φ=90°: (a) 3 GHz, (b) 5 GHz and (c) 7 GHz; H-plane cut, at φ=0°: (d) 3 GHz, (e) 5 GHz and (f) 7 GHz [46]. Reproduced, with permission, from IIL, Applied Materials Today; published by Elsevier, 2020

Metrology and characterisation of wearable antennas require two validation approaches due to the dynamic environment of being worn. The first one is the same as for conventional antennas that cover fundamental parameters in order to verify the performance correlation between fabricated and simulated designs. These features include scattering parameters with the insertion losses, gain, effi-ciency and radiation patterns.

Second, wearable antennas need to face special conditions due to the fact of being worn by a person. Different measurement methods are available for vali-dating the antenna to be worn such as robustness, durability, bending and crum-pling effects. Environmental factors like temperature or RH alter the physical properties of the materials and hence the antenna behaviour, for example shifting in frequency. The proximity of human body parts has an impact as well reducing the efficiency of the system because they are a lossy medium, affecting the radiation properties overall. Frequency detune is another important consequence of this specific situation, where an antenna is placed nearby a person. Therefore, numer-ical and experimental human–tissue phantoms have been developed at different frequencies in order to develop accurate and practical wearable antennas. However, developing a standard measurement method is complicated due to the variety and complexity of the human body.

Acknowledgements

References

[1] Hao Y. and Foster R. 'Wireless body sensor networks for health-monitoring applications'. *Physiological Measurement*, 2008, vol. 28(11), pp. 27–56.

[2] Cotton S.L., Scanlon W.G., and Madahar B.K. 'Millimeter-wave soldier-to-soldier communications for covert battlefield operations'. *IEEE Communications Magazine*, 2009, vol. 47(10), pp. 72–81.

[3] Pellegrini A., Brizzi A., Zhang L., *et al.* 'Antennas and propagation for body-centric wireless communications at millimeter-wave frequencies: A review [wireless corner]'. *IEEE Antennas and Propagation Magazine*, 2013, vol. 55(4), pp. 262–287.

[4] Rappaport T.S., Sun S., Mayzus R., *et al.* 'Millimeter wave mobile com-munications for 5G cellular: It will work!'. *IEEE Access*, 2013, vol. 1, pp. 335–349.

[5] Yang Z., Pathak P.H., Zeng Y., Liran X., and Mohapatra P. 'Monitoring vital signs using millimeter wave'. *Proceedings of the IEEE MobiHoc'16*, 2016, pp. 211–220.

[6] Zeng Y., Pathak P.H., Yang Z., and Mohapatra P. 'Human tracking and activity monitoring using 60 GHz mm-wave'. *15th ACM/ IEEE International*

Conference on Information Processing in Sensor Networks (IPSN), Vienna, 2016, pp. 1–2.

[7]   Chahat N., Tang A., Guraliuc A., Zhadobov M., Sauleau R., and Valerio G. 'Antennas, phantoms, and body-centric propagation at millimeter-waves' in Werner D.H. and Jiang Z.H. (eds.). *Electromagnetics of Body Area Networks: Antennas, Propagation, and RF Systems*, Hoboken, NJ, Wiley, 2016, pp. 205–259.

[8]   Leduc C. and Zhadobov M. 'Impact of antenna topology and feeding tech-nique on coupling with human body: Application to 60-GHz antenna arrays'. *IEEE Transactions on Antennas and Propagation*, 2017, vol. 65(12), pp. 6779–6787.

[9]   Nechayev Y.I., Wu X., Constantinou C., and Hall P.S. 'Millimetre-wave path loss variability between two body-mounted monopole antennas'. *IET Microwaves, Antennas & Propagation*, 2013, vol. 7(1), pp. 1–7.

[10] Hall P.S. and Hao Y. *Antennas and Propagation for Body-Centric Wireless Communications*, Norwood, MA, Artech House, 2006.

[11] Conway G.A. and Scanlon W.G. 'Antennas for over-body-surface commu-nication at 2.45 GHz'. *IEEE Transactions on Antennas and Propagation*, 2009, vol. 57(4), pp. 844–855.

[12] Chahat N., Zhadobov M., Le Coq L., Alekseev S.I., and Sauleau R. 'Characterization of the interactions between a 60-GHz antenna and the human body in an off-body scenario'. *IEEE Transactions on Antennas and Propagation*, 2012, vol. 60(12) pp. 5958–5965.

[13] Chahat N., Zhadobov M., Muhammad S.A., Le Coq L., and Sauleau R. '60-GHz textile antenna array for body-centric communications'. *IEEE Transactions on Antennas and Propagation*, 2013, vol. 61(4), pp. 1816–1824.

[14] Chahat N., Zhadobov M., Le Coq L., and Sauleau R. 'Wearable end-fire textile antenna for on-body communications at 60 GHz'. *IEEE Antennas and Wireless Propagation Letters*, 2012, vol. 11, pp. 799–802.

[15] Wu X.Y., Akhoondzadeh L., and Hall P.S. 'Printed Yagi-Uda array for on-body communication channels at 60 GHz'. *Microwave and Optical Technology Letters*, 2011, vol. 53(12), pp. 2728–2730.

[16] Jilani S.F. and Alomainy A. 'Millimeter-wave conformal antenna array for 5G wireless applications'. *IEEE AP-S Symposium*, San Diego, CA, USA, 2017.

[17] Jilani S.F. and Alomainy A. 'An inkjet-printed MMW frequency reconfi-gurable antenna on a flexible PET substrate for 5G wireless systems'. *LAPC IET*, Loughborough, UK, 2017, pp. 13–14.

[18] Ur-Rehman M., Malik N.A., Yang X., Abbasi Q.H., Zhang Z., and Zhao N. 'A low profile antenna for millimeter-wave body-centric applications'. *IEEE Transactions on Antennas and Propagation*, 2017, vol. 65(12), pp. 6329–6337.

[19] Simorangkir R.B.V.B., Yang Y., and Esselle K.P. 'Performance of embroi-dered higher-order mode antennas with different stitching patterns'. *11th European Conference on Antennas and Propagation (EUCAP)*, Paris, 2017, pp. 177–180.

[20] Yoshikawa T. and Maeda T. 'Embroidered wideband wearable slot antennas using conductive yarn with different yarn-spacing densities'. *International Workshop on Electromagnetics: Applications and Student Innovation Competition (iWEM)*, Hsinchu, 2015, pp. 1–2.

[21] Elobaid H.A.E., Abdul Rahim S.K., Himdi M., Castel X., and Abedian Kasgari M. 'A transparent and flexible polymer-fabric tissue UWB antenna for future wireless networks'. *IEEE Antennas and Wireless Propagation Letters*, 2017, vol. 16, pp. 1333–1336.

[22] Khan S., Lorenzelli L., and Dahiya R.S. 'Technologies for printing sensors and electronics over large flexible substrates: A review'. *IEEE Sensors Journal*, 2015, vol. 15(6), pp. 3164–3185.

[23] Shamim A. '3D inkjet printed flexible and wearable antenna systems'. *International Symposium on Antennas and Propagation (ISAP)*, Phuket, 2017, pp. 1–2.

[24] Hettak K., Ross T., James R., Momciu A., and Wight J. 'Flexible poly-ethylene terephthalate-based inkjet printed CPW-fed monopole antenna for 60 GHz ISM applications'. *European Microwave Conference*, Nuremberg, 2013, pp. 1447–1450.

[25] Maza A.R., Cook B., Jabbour G., and Shamim A. 'Paper-based inkjet-printed ultra-wideband fractal antennas'. *IET Microwaves, Antennas & Propagation*, 2012, vol. 6(12), pp. 1366–1373.

[26] Olkkonen J., Lehtinen K., and Erho T. 'Flexographically printed fluidic struc-tures in paper'. *Analytical Chemistry*, 2010, vol. 82(24), pp. 10246–10250.

[27] Eshkeiti A., Reddy A.S.G., Emamian S., *et al.* 'Screen printing of multi-layered hybrid printed circuit boards on different substrates'. *IEEE Transactions on Components, Packaging and Manufacturing Technology*, 2015, vol. 5(3), pp. 415–421.

[28] Xiao G.G., Zhang Z, Lang S., and Tao Y.'Screen printing RF antennas'. *17th International Symposium on Antenna Technology and Applied Electromagnetics (ANTEM)*, Montreal, QC, 2016, pp. 1–2.

[29] Jilani S.F., Rahimian A., Alfadhl Y., and Alomainy A. 'Low-profile flexible frequency-reconfigurable millimetre-wave antenna for 5G applications'. *Flexible and Printed Electronics – IOPscience*, 2018, vol. 3(3), 5003.

[30] Fang Y., Hester J.G.D., Su W., Chow J.H., Sitaraman S.K., and Tentzeris M. M. 'A bio-enabled maximally mild layer-by-layer Kapton surface mod-ification approach for the fabrication of all-inkjet-printed flexible electronic devices'. *Nature Scientific Reports*, 2016, vol. 6, 39909.

[31] Watson D.E., Ng, J.H., and Desmulliez M.P.Y. 'Additive photolithography based process for metal patterning using chemical reduction on surface modified polyimide'. *18th European Microelectronics & Packaging Conference*, Brighton, 2011, pp. 1–7.

[32] Rabbani M.S. and Ghafouri-Shiraz H. 'Liquid crystalline polymer substrate-based THz microstrip antenna arrays for medical applications'. *IEEE Antennas and Wireless Propagation Letters*, 2017, vol. 16, pp. 1533–1536.

[33] Jilani S.F., Munoz M.O., Abbasi Q.H., and Alomainy A. 'Millimeter-wave liquid crystal polymer based antenna array for conformal 5G applications'. *IEEE Antennas and Wireless Propagation Letters*, 2019, vol. 18(1), pp. 84–88.

[34] Jilani S.F., Aziz A.K., Abbasi Q.H., and Alomainy A. 'Ka-band flexible Koch fractal antenna with defected ground structure for 5G wearable and conformal applications'. *IEEE 29th Annual International Symposium on Personal, Indoor and Mobile Radio Communications (PIMRC 2018)*, 2018, pp. 361–364.

[35] Khaleel H.R. 'Design and fabrication of compact inkjet printed antennas for integration within flexible and wearable electronics'. *IEEE Transactions on Components, Packaging and Manufacturing Technology*, 2014, vol. 4(10), pp. 1722–1728.

[36] Jilani S.F., Falade O.P., Wildsmith T., Reip P., and Alomainy A. 'A 60-GHz ultra-thin and flexible metasurface for frequency-selective wireless appli-cations'. *Applied Sciences, Special Issue: Frequency Selective Surfaces*, 2019, vol. 9(5), 945.

[37] Falade O.P., Jilani S.F., Ahmed A.Y., *et al.* 'Design and characterisation of a screen-printed millimetre-wave flexible metasurface using copper ink for communication applications'. *Flexible and Printed Electronics–IOPscience*, 2018, vol. 3(4), 5005.

[38] Guo X., Ying H., Weidong P., Wenging K., Leidong M., and Yugang Z. 'Flexible and deformable monopole antenna based on silver nanoparticles for wearable electronics'. *Nanoscience Nanotechnology Letters*, 2017, vol. 9 (11), pp. 1632–1638.

[39] Guo X., Hang Y., Xie Z., Wu C., Gao L., and Liu C. 'Flexible and wearable 2.45 GHz CPW-fed antenna using inkjet-printing of silver nanoparticles on PET substrate'. *Microwave Optical Technology Letters*, 2017, vol. 59(1), pp. 204–208.

[40] Guo X., Huang Y., Wu C., *et al.* 'Flexible and reversibly deformable radio-frequency antenna based on stretchable SWCNTs/PANI/ Lycra conductive fabric'. *Smart Materials and Structures-IOPscience*, 2017, vol. 26(10), 5036.

[41] Kumar A., Saghlatoon H., La T.G., *et al.* 'A highly deformable conducting traces for printed antennas and interconnects: Silver/ fluoropolymer compo-site amalgamated by triethanolamine'. *Flexible and Printed Electronics –IOPscience*, 2017, vol. 2(4), 5001.

[42] Wang Z., Volakis J.L., and Kiourti A. 'Chapter 10: Embroidered antennas for communication systems' in *Electronic Textiles*, Amsterdam, Elsevier, 2015, pp. 201–237.

[43] Corchia L., Monti G., and Tarricone L. 'Durability of wearable antennas based on nonwoven conductive fabrics: Experimental study on resistance to washing and ironing'. *International Journal of Antennas and Propagation*, 2018, pp. 1–8, Article ID 2340293.

[44] Yang X., Huang Y., Dai Z., Barber J., Wang P., and Lu N. 'Cut-and-paste: Method for the rapid prototyping of soft electronics'. *Science China Technological Sciences*, 2019, vol. 62(2), pp. 199–208.

[45] Ibanez-Labiano I. and Alomainy A. 'Dielectric characterization of non-conductive fabrics for temperature sensing through resonating antenna structures'. *MDPI Materials*, 2020, vol. 13(6), pp. 1271.

[46] Ibanez-Labiano I., Ergoktas M.S., Kocabas C., Toomey A., Alomainy A., and Ozden-Yenigun E. 'Graphene-based soft wearable antennas'. *Applied Materials Today*, 2020, vol. 20, 100727.

[47] Mazzinghi A., Blaschi L., and Freni A. '3D printed low cost high gain antennas'. *IEEE Antennas and Wireless Propagation Letters*, 2018, vol. 1(1).

[48] Pethig R. 'Dielectric properties of body tissues'. *Clinical Physics and Physiological Measurement*, 1987, vol. 8(4A), pp. 5–12.

[49] Gabriel C. 'Compilation of the dielectric properties of body tissues at RF and microwave frequencies'. *Physics*, 1996.

[50] Institute for Applied Physics. Dielectric properties of body tissues in the frequency range 10 Hz–100 GHz Italian National Research Council [online]. Available from: http://niremf.ifac.cnr.it/tissprop/ [Accessed 4 March 2021].

[51] Tell R.A. 'Microwave energy absorption in tissue'. *EPA, Twinbrook Research Laboratory Technical Report*, 1972.

[52] Ito, K. 'Numerical and experimental human body phantoms'. *IET Seminar on Antennas and Propagation for Body-Centric Wireless Communications*, 2007, pp. 6–12.

[53] CST Microwave Studio [online]. Available from: https://www.3ds.com/products-services/simulia/products/cst-studio-suite/ [Accessed 4 March 2021].

[54] Abd Rahman N.H., Yamada Y., and Amin Nordin M.S. 'Analysis on the effects of the human body on the performance of electro-textile antennas for wearable monitoring and tracking application'. *MDPI Materials*, 2019, vol. 12(10), 1636.

[55] Federal Communications Commission. *Evaluating compliance with FCC guidelines for human exposure to radiofrequency electromagnetic fields*. Supplement C to bulletin 65, 2001.

[56] Kanda M.Y., Flallen M., Chou C.K., and Balzano Q. 'Formulation and characterization of tissue equivalent liquids used for RF densitometry and dosimetry measurements'. *IEEE Transactions on Microwave Theory and Techniques*, 2004, vol. 52(8), pp. 2046–2056.

[57] Takimoto T., Onishi T., Saito K., Takahashi M., Uebayashi S., and Ito K. 'Characteristics of biological tissue equivalent phantoms applied to UWB communications'. *Electronics Communications in Japan (Part I: Communications)*, 2007, vol. 90(5), pp. 48–55.

[58] Garrett J. and Fear E. 'Stable and flexible materials to mimic the dielectric properties of human soft tissues'. *IEEE Antennas Wireless and Propagation Letters*, 2014, vol. 13, pp. 599–602.

[59] Conway G.A. and Scanlon W.G. 'Antennas for over-body-surface commu-nication at 2.45 GHz'. *IEEE Transactions on Antennas Propagation*, 2009, vol. 57(4), pp. 844–855, 10560828.

[60] Giddens H., Paul D.L., Hilton G., and McGeehan J.P. 'Numerical and experimental evaluation of phantoms for off-body wireless communica-tions'. *Loughborough Antennas & Propagation Conference*, 2011, pp. 1–4.

[61] Guy A.W. 'Analysis of electromagnetic fields induced in biological tissues by the thermographic studies on equivalent phantom models'. *IEEE Transactions on Microwave Theory and Techniques*, 1971, vol. 19(2), pp. 205–214.

[62] Okano Y., Ito K., Ida I., and Takahashi M. 'The SAR evaluation method by a combination of thermographic experiments and biological tissue-equivalent phantoms'. *IEEE Transactions on Microwave Theory and Techniques*, 2000, vol. 48(11), pp. 2094–2103.

[63] SPEAG [online]. Available from: https://speag.swiss/ [Accessed 4 March 2021].

[64] Li Y. and Dai X.Q. *Biomechanical Engineering of Textiles and Clothing*, 1st edn. Cambridge: Woodhead Publishing, 2006, p. 428.

[65] Castano L. and Flatau A. 'Smart fabric sensors and e-textile technologies: A review'. *Smart Materials Structures*, 2014, vol. 23, 053001.

[66] Pekka S., Mikko K., and Yahya S. 'Textile antennas: Effects of antenna bending on radiation pattern and efficiency'. *Antennas and Propagation Society International Symposium*, San Diego, CA, 5–11 July 2008, 10219545.

[67] Salonen P. and Rahmat-Samii Y. 'Textile antennas: Effects of antenna bending on input matching and impedance bandwidth'. *First European Conference on Antennas and Propagation*, Nice, 2006, pp. 1–5.

[68] Elias N.A., Samurai N.A., and Rahim M.K.A. 'Analytical study of energy absorption in human body due to bendable behaviour of textile antenna' in Zainal H. (ed.). *Theory and Applications of Applied Electromagnetics*. Lecture Notes in Electrical Engineering Series, no. 344, 2015, pp. 329–337.

[69] Xu B., Eike R.J., Cliett A., Ni L., Cloud R., and Li Y. 'Durability testing of electronic textile surface resistivity and textile antenna performance'. *Textile Research Journal*, 2019, vol. 89(18), pp. 3708–3721.

[70] Fernandes D.E.D., Marcos J.S., Maslovski S.I., and Silveirinha, M.G. 'Measurement of the specific absorption rate using a single electric field sensor'. *IEEE EUROCON – International Conference on Computer as a Tool*, 2011, pp. 1–4.

[71] Wang Z., Lin J.C., Mao W., Liu W., Smith M.B., and Collins C.M. 'SAR and temperature: Simulations and comparison to regulatory limits for MRI'. *Journal of Magnetic Resonance Imaging*, 2007, vol. 26(2), pp. 437–441.

[72] ICNIRP. 'Guidelines for limiting exposure to electromagnetic fields (100 kHz to 300 GHz)'. *Health Physics*, 2020, vol. 18(5), pp. 483–524.

[73] Klancnik M., Rijavec B., Pivar M., and Muck D. 'Influence of printing material and printing ink layer on RFID antenna operation'. *Tekstilec*, 2018, vol. 61(3), pp. 162–170.

[74] Lilja J., Salonen P., Kaija T., and Maagt P. 'Design and manufacturing of robust textile antennas for harsh environments'. *IEEE Transactions on Antennas and Propagation*, 2012, vol. 60(9), pp. 4130–4140.

[75] Branimir I., Goran G., and Davor B. 'Performance of wearable antenna exposed to adverse environmental conditions'. *21st International Conference on Applied Electromagnetics and Communications*, Dubrovnik, Croatia, 14–16 October 2013, paper no. 13990440.

[76] Moraru A., Ursachi C., and Helerea E. 'A new washable UHF RFID tag: Design, fabrication, and assessment'. *MDPI Sensors*, 2010, vol. 20(12), 3451.

[77] Simorangkir R.B.V.B., Le D., Björninen T., Sayem A.S.M., Zhadobov M., and Sauleau R. 'Washing durability of PDMS-conductive fabric composite: Realizing washable UHF RFID tags'. *IEEE Antennas and Wireless Propagation Letters*, 2019, vol. 18(12), pp. 2572–2576.

[78] Scarpello M.L., Kazani I., Hertleer C., Rogier H., and Ginste D.V. 'Stability and efficiency of screen-printed wearable and washable antennas'. *IEEE Antennas and Wireless Propagation Letters*, 2012, vol. 11, pp. 838–841.

[79] Gorgutsa S., Bachus K., LaRochelle S., Oleschuk R.D., and Messaddeq Y. 'Washable hydrophobic smart textiles and multi-material fibers for wireless communication'. *Smart Materials and Structures*, 2016, vol. 25(11), 115027.

[80] Carla H., Annelien L., Hendrik R., and Van Langenhove L. 'Influence of relative humidity on textile antenna performance'. *Textile Research Journal*, 2009, vol. 80(2), pp. 177–183.

[81] Yilmaz S. 'The geometric resistivity correction factor for several geome-trical samples'. *Journal of Semiconductors*, 2015, vol. 36(8), 082001.

[82] Sankaralingam S. and Gupta B. 'Determination of dielectric constant of fabric materials and their use as substrates for design and development of antennas for wearable applications'. *IEEE Transactions on Instrumentation and Measurement*, 2012, vol. 59(12), pp. 3122–3130.

[83] Lesnikowski J. 'Dielectric permittivity measurement methods of textile substrate of textile transmission lines'. *Przeglad Elektrotechniczny (Electrical Review)*, 2012, R.88 NR-3a.

[84] Morton W.E. and Hearle J.W.S. *Physical Properties of Textile Fibres*, 4th edn. Cambridge: Woodhead Publishing Limited and CRC Press LLC, 2008.

[85] Lin X., Seet B.C., and Joseph F. 'Wearable humidity sensing antenna for BAN applications over 5G networks'. *IEEE 19th Wireless and Microwave Technology Conference (WAMICON)*, Sand Key, FL, 2018, pp. 1–4.

[86] Jang J.H. and Han J.I. 'Cylindrical relative humidity sensor based on poly-vinyl alcohol (PVA) for wearable computing devices with enhanced sensitivity'. *Sensors Actuators A: Physical*, 2017, vol. 261, pp. 268–273.

[87] Chang K., Kim Y.H., Kim Y.J., and Yoon Y.J. 'Functional antenna integrated with relative humidity sensor using synthesised polyimide for passive RFID sensing'. *Electronics Letters*, 2007, vol. 43(5), pp. 7–8.

[88] Controltecnica-CTS. Climatic test chambers [online]. Available from: https://www.cts-clima.com/en/climatic-testing/climatic-test-chambers.html [Accessed 4 March 2021].

[89] Aboufoul T., Parini C., Chen X., and Alomainy A. 'Pattern-reconfigurable planar circular ultra-wideband monopole antenna'. *IEEE Transactions on Antennas and Propagation*, 2013, vol. 61(10), pp. 4973–4980.

[90] Aboufoul T., Ali K., Alomainy A., and Parini C. 'Combined pattern and frequency reconfiguration of single-element ultra-wideband monopole antenna for cognitive radio devices'. *7th European Conference on Antennas and Propagation (EuCAP)*, 2013, pp. 932–936.

[91]   Andrade A.d.C., Fonseca I.P., Jilani S.F., and Alomainy A. 'Reconfigurable textile-based ultra-wideband antenna for wearable applications'. *10th European Conference on Antennas and Propagation (EuCAP)*, 2016, pp. 1–4.

[92]   Singh J., Rani E.S., and Singh E.M. 'Design of microstrip patch antenna array for traffic speed detector application'. *5th International Conf. on Advanced Computing & Communication Technologies (ACCT)*, 2015, pp. 4–7.

[93]   Holub A. and Polivka M. 'Collinear microstrip patch antenna' in *Passive Microwave Components and Antennas*. London: InTech, 2010, Ch. 24, pp. 513–530.

[94]   Polivka M., Holub A., and Mazanek M. 'Collinear microstrip patch antenna'. *Radioengineering*, 2005, vol. 14(4), pp. 40–42.

[95]   Solbach K. 'Microstrip-Franklin antenna'. *IEEE Transactions on Antennas and Propagation*, 1982, vol. 30(4), pp. 773–775.

[96]   Wang P.P., Antoniades M.A., and Eleftheriades G.V. 'An investigation of printed Franklin antennas at X-band using artificial (metamaterial) phase-shifting lines'. *IEEE Transactions on Antennas and Propagation*, 2008, vol. 56(10), pp. 3118–3128.

[97]   Chang S.H., Liao W.J., Peng K.W., and Hsieh C.Y. 'A Franklin array antenna for wireless charging applications'. *PIERS*, 2010, vol. 6(4), pp. 340–344.

[98]   Azlan A.A., Ali M.T., Awang M.Z., and Jamlos M.F. 'A simulation of single patch antenna with phantom tissue for ISM band'. *National Conference on Medical at Center of Medical Electronic Politeknik Shah Alam*, 2014.

[99]   Antennas & Electromagnetics Research Group, Queen Mary University of London. Available from: http://antennas.eecs.qmul.ac.uk/facilities/antenna-measurement-laboratory/ [Accessed 4 March 2021].